Title

Solvent Assisted Excited State Proton Transfer in Indigo Carmine Investigated by Two-Dimensional Electronic-Vibrational Spectroscopy

Authors

Roy, PP

Shee, J

Arsenault, EA

et al.

Publication Date

2020-11-16

DOI

10.1364/up.2020.m4b.8

Peer reviewed

Biochemistry

Article

Cite This: Biochemistry 2020, 59, 594−604

pubs.acs.org/biochemistry

Interconnection of the Antenna Pigment 8-HDF and Flavin Facilitates Red-Light Reception in a Bifunctional Animal-like Cryptochrome

Sabine Oldemeyer,*[,†,‡] Andrew Z. Haddad,[§] and Graham R. Fleming[†,‡,∥]

[†]Department of Chemistry, University of California, Berkeley, California 94720, United States

[‡]Molecular Biophysics and Integrated Bioimaging Division, Lawrence Berkeley National Laboratory, Berkeley, California 94720, United States

[§]Energy Technologies Area, Lawrence Berkeley National Laboratory, Berkeley, California 94720, United States

[∥]Kavli Energy Nanoscience Institute, Berkeley, California 94720, United States

Supporting Information

ABSTRACT: Cryptochromes are ubiquitous flavin-binding light sensors closely related to DNA-repairing photolyases. The animal-like cryptochrome *Cra*CRY from the green alga *Chlamydomonas reinhardtii* challenges the paradigm of cryptochromes as pure blue-light receptors by acting as a (6−4) photolyase, using 8-hydroxy-5-deazaflavin (8-HDF) as a light-harvesting antenna with a 17.4 Å distance to flavin and showing spectral sensitivity up to 680 nm. The expanded action spectrum is attributed to the presence of the flavin neutral radical ($FADH^{\bullet}$) in the dark, despite a rapid $FADH^{\bullet}$ decay observed *in vitro* in samples exclusively carrying flavin. Herein, the red-light response of *Cra*CRY carrying flavin and 8-HDF was studied, revealing a 3-fold prolongation of the $FADH^{\bullet}$ lifetime in the presence of 8-HDF. Millisecond time-resolved ultraviolet−visible spectroscopy showed the red-light-induced formation and decay of an absorbance band at 458 nm concomitant with flavin reduction. Time-resolved Fourier transform infrared (FTIR) spectroscopy and density functional theory attributed these changes to the deprotonation of 8-HDF, challenging the paradigm of 8-HDF being permanently deprotonated in photolyases. FTIR spectra showed changes in the hydrogen bonding network of asparagine 395, a residue suggested to indirectly control flavin protonation, indicating the involvement of N395 in the stabilization of $FADH^{\bullet}$. Fluorescence spectroscopy revealed a decrease in the energy transfer efficiency of 8-HDF upon flavin reduction, possibly linked to 8-HDF deprotonation. The discovery of the interdependence of flavin and 8-HDF beyond energy transfer processes highlights the essential role of the antenna, introducing a new concept enabling *Cra*CRY and possibly other bifunctional cryptochromes to fulfill their dual function.

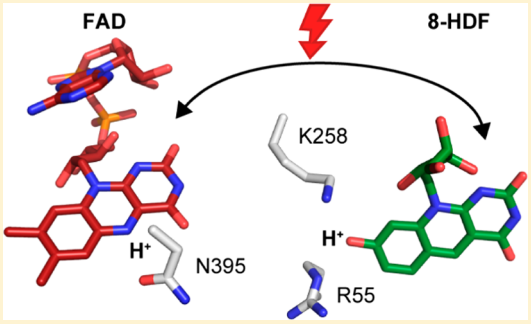

Cryptochromes constitute a diverse group of sensory photoreceptors present in all three kingdoms of life and are known to regulate a wide range of processes.[1−5] They form the cryptochrome/photolyase family, together with photolyases, enzymes responsible for repairing ultraviolet (UV)-light-induced DNA lesions, either cyclobutane-pyrimidine dimers (CPD)[6] or pyrimidine-(6−4)-pyrimidone photoadducts, (6−4)PP.[7] Members of this protein family share the highly conserved photolyase homology region (PHR) comprising 500 residues.[1]

The C-terminal α-helical domain of the PHR harbors the light-sensing flavin adenine dinucleotide (FAD) chromophore, whereas the N-terminal α/β domain in some cases binds a light-harvesting pigment noncovalently, commonly known as an antenna chromophore. Known antenna chromophores include 5,10-methenyltetrahydrofolate (MTHF),[8,9] 7,8-dimethyl-8-hydroxy-5-deazaflavin (8-HDF),[10−12] flavin mononucleotide (FMN),[13] 6,7-dimethyl-8-ribityllumazine (DMLR),[14] and FAD in its fully oxidized state (FAD_{ox}).[15] In many cryptochromes and photolyases, a C-terminal extension (CCT) with a highly varying amino acid composition and length is present and was found in plant and insect cryptochromes to be involved in signaling.[16,17]

The cryptochrome subfamily further diversifies into animal types I and II, plant CRYs, and DASH cryptochromes (*Drosophila*, *Arabidopsis*, *Synechocystis*, and *Homo*).[18,19] The group of animal type II cryptochromes is closely related to (6−4) photolyases and includes the animal-like cryptochrome *Cra*CRY or, for short, aCRY, from the green algae *Chlamydomonas reinhardtii*.[20] Strikingly, aCRY challenges the paradigm of cryptochromes being exclusively blue-light receptors, as it responds *in vivo* to red light up to 680 nm by

Received: September 24, 2019
Revised: December 17, 2019
Published: December 17, 2019

DOI: 10.1021/acs.biochem.9b00875
Biochemistry 2020, 59, 594−604

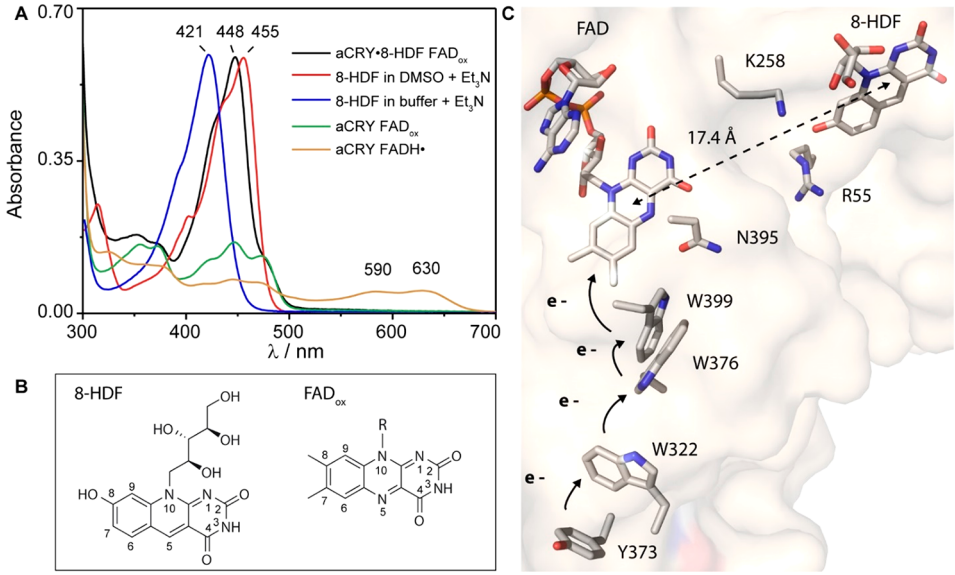

Figure 1. (A) Absorbance of aCRY·8-HDF is compared to aCRY carrying FAD$_{ox}$ or FADH$^{\bullet}$, and 8-HDF in different solvents. aCRY·8-HDF has a maximum at 448 nm and a shoulder at 473 nm showing the noncovalent binding of 8-HDF and FAD$_{ox}$, respectively. (B) Chemical structures of FAD$_{ox}$ and protonated 8-HDF. (C) Tyrosine 373 and the tryptophans 322, 376, and 399 form the electron transfer tetrad that is responsible for flavin reduction. Asparagine 395 is proposed to indirectly control the deprotonation of FADH$^{\bullet}$. Lysine 258 and arginine 55 are suggested to be involved in the deprotonation of 8-HDF. The protein structure is taken from ref 29 (Protein Data Bank entry 6FN2).

altering transcript levels for proteins involved in processes such as cell cycle control and chlorophyll and carotenoid biosynthesis.[20] As opposed to plant cryptochromes, where the oxidized flavin (FAD$_{ox}$) is present,[21,22] the broadened spectral sensitivity observed in aCRY is rationalized by the noncovalent binding of the flavin neutral radical (FADH$^{\bullet}$) in the dark form of the receptor (Figure 1A).[20] The FADH$^{\bullet}$ absorption spectrum was found to be in agreement with the action spectrum of aCRY *in vivo*, and structural rearrangements in the protein moiety of aCRY were found only upon formation of the anionic fully reduced state (FADH^{-}) as revealed by Fourier transform infrared (FTIR) spectroscopy and hydrogen/deuterium exchange mass spectrometry on aCRY.[23−25]

In contrast to other cryptochromes, the lifetime of the FADH$^{\bullet}$ state *in vitro* is not influenced by oxygen levels[26−28] but is strongly sensitive to alterations of the pH. At a pH of 6.9, a lifetime of 1340 s was reported.[23] Neighboring amino acids were proposed to control the pH sensitivity by acting as proton donors.[23] Franz et al. suggested that the asparagine 395 (N395) in the proximity of FAD (Figure 1C) might function as a gatekeeper for a solvent-dependent deprotonation of FADH$^{\bullet}$ and thus indirectly regulates the radical's stability.[29] However, an explanation for the short lifetime of the FADH$^{\bullet}$ *in vitro* as opposed to its permanent presence *in vivo* is not yet available.

In addition to the protein's structural response, it was found that in aCRY tyrosine 373 (Y373) is oxidized in ∼800 ps[30] and forms a long-lived tyrosyl radical (TyrO$^{\bullet}$) with a lifetime of 2.6 s upon red-light illumination.[24,31] TyrO$^{\bullet}$ is stabilized by the formation of a $\pi-\pi$ stack with the neighboring tryptophan 322 (W322).[32] Both Y373 and W322 are part of the conserved redox tetrad (Figure 1C) and are essential for the successful photoreduction.

Interestingly, aCRY was only recently found to have maintained the ability to repair (6−4)PP DNA lesions *in vivo* and to carry the noncovalently bound antenna pigment 8-HDF possibly deprotonated at the 8-hydroxyl group[29] that has a pK_a value of 6.3[33] (Figure 1B). The deprotonation was rationalized by the presence of positively charged residues lysine 258 (L258) and arginine 55 (R55) next to the 8-hydroxyl group[10,29] (Figure 1C) as well as the red-shifted absorbance maximum at 448 nm, which is similar to spectra previously found for other 8-HDF-binding photolyases.[10,12,34] In these enzymes, the red-shifted absorbance as opposed to the pigment's absorbance maximum in aqueous solution at 421 nm (Figure 1A) was explained by a negative solvatochromic effect exhibited by charged species in a nonpolar environment such as the protein matrix.[35] Previous experiments investigating the red-light response of aCRY *in vitro* were conducted exclusively on samples without the antenna pigment 8-HDF. The recent discovery of the noncovalent binding of 8-HDF in aCRY raises the question of whether it solely serves to increase DNA repair efficiency in the protein's role as a photolyase or whether it may also have an impact on aCRY function as a red-light sensor especially with regard to the formation of the stable tyrosyl radical. In this study, we address this question through the use of millisecond time-resolved ultraviolet−visible (UV−vis) spectroscopy, millisecond time-resolved infrared spectroscopy, quantum chemical calculations, and fluorescence spectroscopy.

MATERIALS AND METHODS

Expression and Purification of aCRY·8-HDF and aCRY.

Wild-type aCRY protein carrying FAD and the antenna chromophore 8-HDF (aCRY·8-HDF) was expressed in *Escherichia coli* BL21(DE3) after the cells had been transformed with pET28a-aCRY and the cofactor plasmid pCDF-His$_6$FbiC that encodes the F0 synthase (7,8-didemethyl-8-hydroxy-5-deazariboflavin synthase) of *Streptomyces coelicolor*. Wild-type aCRY without 8-HDF carrying only FAD (aCRY) was expressed in *E. coli* BL21(DE3) subsequent to the transformation of the cells with pET28a-aCRY. These procedures and the purification of aCRY·8-HDF and aCRY were conducted following published protocols.[20,36] The

DOI: 10.1021/acs.biochem.9b00875
Biochemistry 2020, 59, 594−604

proteins were dissolved in a 50 mM sodium phosphate buffer (pH 7.0) with 100 mM NaCl and 20% (v/v) glycerol after final dialysis. As a control for sample homogeneity, a fraction of the sample was further purified using size exclusion chromatography (Supporting Information).

The chromophore occupancy was determined before and after this additional size exclusion chromatography by spectrally decomposing an absorbance spectrum of aCRY·8-HDF according the Beer–Lambert law[37] given in eq 1.

$$A = lc\varepsilon \quad (1)$$

where the absorbance A is given by the product of path length l, concentration c, and molar extinction coefficient ε. The flavin concentration was calculated using the molar extinction coefficient of oxidized flavin at 450 nm (11300 M^{-1} cm^{-1})[38] after scaling an absorbance spectrum of aCRY to the flavin shoulder at 476 nm in the aCRY·8-HDF spectrum (Figure S1). After subtraction of the flavin absorbance portion from the aCRY·8-HDF spectrum, the molar extinction coefficient of 8-HDF at 448 nm of 37500 M^{-1} cm^{-1}[35] was used to obtain the 8-HDF concentration. To determine the protein concentration, an absorbance spectrum of a 3-fold dilution of the aCRY·8-HDF sample was generated and both flavin and 8-HDF contributions were subtracted from the absorbance at 280 nm. Using the molar extinction coefficient of the aCRY protein matrix at 280 mn (107830 M^{-1} cm^{-1}),[39] the overall protein concentration and chromophore occupancy were determined.

UV–Vis Spectroscopy and Kinetic Experiments. UV–vis spectra were recorded using a UV-2450 spectrometer (Shimadzu). The concentrations of each of three independent aCRY·8-HDF and aCRY samples were adjusted to an A_{448} of 0.6 and an A_{450} of 0.3, respectively, for long-term kinetics. The flavin neutral radical was generated by illuminating aCRY·8-HDF and aCRY for 3 and 1 s, respectively, using 473 and 451 nm light-emitting diodes (LEDs) (Luxeon Star, Lumileds) with intensities of 32 mW/cm^2 at the sample and a full width at half-maximum (fwhm) of 15 nm. The decay of the flavin neutral radical was recorded at 630 nm subsequent to the illumination.

Millisecond Time-Resolved UV–Vis Spectroscopy. Three independent samples with a concentration adjusted to an optical density of 0.6 at 448 nm were measured in an HR2000+ spectrometer (Ocean Optics) in a 2 mm × 10 mm fluorescence cuvette (Helma). The DH-2000-BAL light source was attenuated by a mesh filter with 35% transmission to prevent photobleaching of the sample with the probe light. Photoconversion was conducted with two LEDs perpendicularly fastened to the sample holder. A 473 nm LED (Luxeon Star, Lumileds) with an intensity of 63 mW/cm^2 (fwhm of 20 nm) and a 632 nm LED (Luxeon Star, Lumileds) with an intensity of 95 mW/cm^2 (fwhm of 15 nm) at the sample were used for 10 or 2 s to generate $FADH^{\bullet}$ and $FADH^{-}$, respectively. During and after illumination, a consistent series of spectra were recorded with an integration time of 2 ms and a time resolution of 44 ms. Difference spectra were calculated and summarized on a logarithmic time scale to improve the signal-to-noise ratio using MATLAB (The Mathworks).

Rapid-Scan FTIR Spectroscopy. Ultrafiltration was conducted using Vivaspin 500 filter devices (Sartorius, 50 kDa cutoff) to concentrate the proteins to a final OD_{447} of ∼25 and an OD_{448} of ∼32 for aCRY and aCRY·8-HDF, respectively. The samples were washed three times with 20 mM sodium phosphate buffer (pH 7.0), 100 mM NaCl, and 1% (v/v) glycerol during centrifugation at 15000g. A droplet of 2.0 μL of the sample solution was placed on a BaF_2 window (20 mm diameter) and kept at 20 °C at atmospheric pressure for ≤20 s for a slight reduction of the water content. An additional BaF_2 window was used to seal the samples forming a well-hydrated film with an absorbance ratio of amide I/water (1650 cm^{-1}) to amide II (1550 cm^{-1}) of 2.4–2.6. An IFS 66/s spectrometer (Bruker) equipped with a photoconductive mercury cadmium telluride (MCT) detector at a spectral resolution of 4 cm^{-1} was used to perform the rapid-scan experiments. The mirror was set in a double-sided, forward–backward mode to a velocity 160 kHz. The difference spectra were obtained with a long wave pass filter (OCLI) cutting off infrared and visible light above 2256 cm^{-1}.

aCRY·8-HDF and aCRY were preilluminated with blue light for 10 s with a 473 nm (aCRY·8-HDF) and 451 nm LEDs (aCRY) equipped with a diffusion disc and yielding intensities of 30 and 32 mW/cm^2 at the sample, respectively. The reference intensity was recorded for 512 scans followed by red-light illumination for 3 s with a 632 nm LED with an intensity of 40 mW/cm^2 at the sample. The first difference spectrum was recorded from 16 to 121 ms with a midpoint of 69 ms after the red-light illumination, and 49 additional spectra were recorded until 1818 s. Subsequently, four (aCRY·8-HDF) or nine (aCRY) single experiments, each time using a fresh and independently prepared sample, were averaged. The experiments were performed at a constant temperature of 10 °C.

Quantum Chemical Calculations. The calculation of normal modes and the optimization of the geometry were performed using density functional theory (DFT) as implemented in Gaussian16 A03[40] using Becke's B3LYP hybrid exchange-correlation functional[41,42] and the 6-311+G-(2d,p) basis set. The B3LYP functional previously yielded results in vibrational frequencies matching the experiment data very well.[42] A single factor of 0.98 was used to scale the frequencies, as it gave excellent results in calculations for flavin.[43] The line spectrum was folded with Lorentzians with a fwhm of 14 cm^{-1} as determined for the homogeneous broadening of flavin bands.[44]

Fluorescence Spectroscopy. Prior to the experiments, all protein samples were purified by size exclusion chromatography via a PD10 column (GE Healthcare) according to the specifications of the manufacturer to remove the unbound chromphore. Samples of aCRY·8-HDF and aCRY were adjusted to the same concentration of FAD_{ox} at 473 nm with an A_{448} of 0.65 and an A_{447} of 0.15, respectively. To ensure the same absorbance of 8-HDF as in the protein sample, the chromophore in 50 mM sodium phosphate buffer (pH 7.0), 100 mM NaCl, 20% (v/v) glycerol, and DMSO each with 0.1% Et_3N was set to A_{421} and A_{455} values of 0.5. A Fluorolog-3 spectrofluorometer (Horiba Jobin Yvon) equipped with a CCD camera was used to record the emission spectra of the samples. For the comparison of the fluorescence intensities of aCRY·8-HDF, aCRY, and 8-HDF solvated in phosphate buffer and DMSO, samples were excited at their absorption maxima at 448, 447, 421, and 455 nm, respectively, with a bandwidth of 5 nm and a detection time of 0.02 s. To generate aCRY·8-HDF with different flavin oxidation states, $FADH^{\bullet}$ was generated upon illumination at 473 nm for 10 s and a permanent stabilization of $FADH^{-}$ was achieved upon addition of 10 μM ascorbic acid and illumination at 473 nm for 40 s. The samples were excited at 432 nm with a detection time of 0.02 s. To test

DOI: 10.1021/acs.biochem.9b00875
Biochemistry 2020, 59, 594–604

the homogeneity of the protein samples, these experiments were repeated with a sample containing 92% and 93% FAD and 8-HDF occupancy, respectively, after an additional size exclusion chromatography step (Figure S2).

Calculation of the Energy Transfer Efficiency in aCRY·8-HDF. The theoretical efficiency of the resonant energy transfer (RET) E was calculated for aCRY·8-HDF with 8-HDF acting as the donor to either FAD_{ox}, $FADH^{\bullet}$, or $FADH^{-}$ as the receptor.

$$E = \frac{R_0^6}{R_0^6 + r^6} \tag{2}$$

The Foerster radius R_0 is the distance at which the energy transfer efficiency between the chromophores is 50%, and r represents the center-to-center distance of the donor−acceptor pair with a value of 17.4 Å as derived from the structure.[29] R_0 was calculated using eq 2:

$$R_0 = 0.211\left[\frac{\kappa^2 \Phi_D J(\lambda)}{n^4}\right]^{1/6} \tag{3}$$

κ^2 is an orientation factor of the chromophores, representing the angle of the transition dipole moments of the donor and acceptor toward each other. An orientation factor of 1.82 was chosen, as calculated for $FADH^{-}$ and 8-HDF in the (6−4) photolyase of *Aspergillus nidulans*.[45] The quantum yield of the donor chromophore in the absence of the acceptor is represented by Φ_D and was determined to be 0.65 for 8-HDF.[46] $J(\lambda)$ is the overlap integral of the molar extinction coefficient of the acceptor in $nm^4\ M^{-1}\ cm^{-1}$ and the normalized emission spectrum of the donor in the absence of the acceptor (Figure S3), and values are listed in Table S1. For the fluorescence spectrum of the donor in the absence of the acceptor, a spectrum of 8-HDF in phosphate buffer was chosen. n is the refractive index with a value of 1.39 for a protein buffer.[47]

RESULTS

The co-expression of wild-type aCRY with a plasmid encoding the F0-synthase revealed 8-HDF to be bound as a potential antenna chromophore in the full-length protein.[29] To investigate the influence of the additional chromophore on the red-light response of the protein, aCRY·8-HDF was successfully expressed and purified carrying both 8-HDF and FAD as confirmed by UV−vis analysis after a final cleansing (Figure 2A). The absorption spectrum of the protein shows a prominent band at 448 nm with a shoulder at 430 nm assigned to 8-HDF. The detection of an additional absorbance band with maxima at 355 and 373 nm, as well as a shoulder at 475 nm verifies the presence of protein-bound flavin in the oxidized state. The occupancies of 8-HDF and FAD_{ox} in aCRY·8-HDF after the complete purification procedure are calculated to be at least 30% and 34%, respectively. After an additional size exclusion chromatography step on a fraction of the sample, aCRY·8-HDF with occupancies of 92% and 93% for FAD and 8-HDF, respectively, was obtained (Figure S1). Fluorescence spectroscopy conducted on samples before and after the additional chromatography step yielded very similar results (Figure S2), showing that in the samples with the lower calculated chromophore occupancy FAD and 8-HDF were binding cooperatively to the same proteins. Therefore, for all of the following experiments, aCRY·8-HDF samples were used without the additional purification step. To study the physiologically relevant red-light response in aCRY·8-HDF, $FADH^{\bullet}$ was generated in the sample via illumination at 473 nm for 10 s. The formation of the characteristic absorbance bands at 590 and 630 nm indicated the successful generation of the neutral radical (Figure 2A).

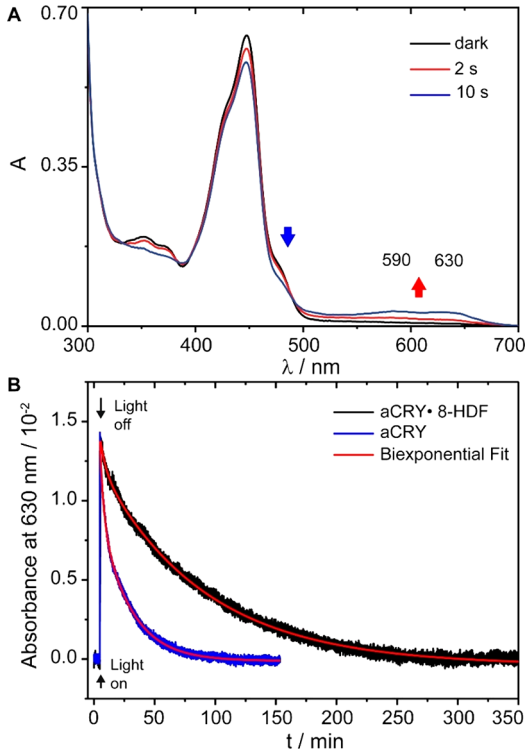

Figure 2. (A) FAD_{ox} is converted to $FADH^{\bullet}$ in aCRY·8-HDF by illumination at 473 nm, shown by the $FADH^{\bullet}$ marker bands at 590 and 630 nm. (B) Comparison of UV−vis long-term kinetics of aCRY·8-HDF and aCRY, scaled by a factor of 0.51. Biexponential fitting yielded time constants of τ_1 = 5225 s (72%) and τ_2 = 284 s (28%) and τ_1 = 1469 s (66%) and τ_2 = 156 s (34%) for aCRY·8-HDF and aCRY, respectively, revealing a 3.5-fold prolongation of the major component of the $FADH^{\bullet}$ lifetime in aCRY·8-HDF relative to aCRY.

Previously, it was found that $FADH^{\bullet}$ decays within an hour to FAD_{ox} at a pH of 6.9 in the dark at 20 °C,[23] constituting a major distinction from the neutral radical's permanent presence *in vivo*.[20] To investigate the effect of the presence of the antenna 8-HDF on the lifetime of $FADH^{\bullet}$ in aCRY·8-HDF, the neutral radical was generated via blue-light illumination at 473 nm for 3 s followed by monitoring the absorbance decay at 630 nm via kinetic measurements at 20 °C and pH 7.0 (Figure 2B). Analysis of the decay curves of three independent samples of aCRY·8-HDF with biexponential fits yielded average time constants of 5225 s (72%, ±510 s) and 284 s (28%, ±21 s). For comparison, the lifetime of $FADH^{\bullet}$ in aCRY was measured in three independent samples under identical conditions except that the sample was illuminated for 1 s at 451 nm. For better visualization, the decay curve of aCRY was scaled by a factor of 0.51. Here, the biexponential fit yielded averaged time constants of 1469 s (66%, ±120 s) and 156 s (34%, ±15 s). Strikingly, the lifetimes of the long and short components in aCRY·8-HDF are 3.5 and 1.8 times longer, respectively, then the lifetime of $FADH^{\bullet}$ found in aCRY.

DOI: 10.1021/acs.biochem.9b00875
Biochemistry 2020, 59, 594−604

Effect of 8-HDF on the Lifetime of TyrO• and FADH⁻ in aCRY·8-HDF. Previously, in aCRY Y373 was found to form an unusually stable tyrosyl radical (TyrO•) with a lifetime of 2.6 s in response to red light, decaying mutually with the FADH⁻.[24] To assess whether the presence of the antenna chromophore influences the stability of the radical, the decay of TyrO• and FADH⁻ after red-light illumination was analyzed at 20 °C on a millisecond time scale. Difference spectra were calculated by subtracting spectra averaged over 1 s subsequent to illumination from spectra prior to illumination (Figure 3A).

In addition to the marker bands of TyrO• and FADH• at 410 and 630 nm, the spectrum of aCRY·8-HDF shows a band at 458 nm (Figure 3A, inset), which is not observed in the difference spectrum of aCRY (Figure 3A), suggesting that it originates from 8-HDF. To analyze the decay of TyrO• and FADH⁻, changes in absorbance at 385−425 and 550−605 nm were integrated and fitted monoexponentially, yielding time constants of 2.0 s for both processes (Figure 3B). TyrO• and FADH⁻ both decay 23% faster than in aCRY (τ = 2.6 s), yielding similar time constants (2.3 s for TyrO• and FADH⁻) as found in the aCRY-C482A mutant,[24] where an alteration in the hydrogen bonding of Y373 was shown to be responsible for the effect.[32] This indicates that the hydrogen bonding network of Y373 is changed in the presence of 8-HDF without disrupting the stabilizing $\pi-\pi$ stacking with tryptophan 322. The absorbance peak at 458 nm attributed to 8-HDF was analyzed by integrating from 450 to 465 nm and fitted monoexponentially (Figure 3C). For this band, a time constant of 1.8 s was determined, only slightly shorter than the values of the TyrO•/FADH⁻ decay constants, implying that the change in the 8-HDF absorption coefficient is linked to the protein's red-light-induced formation and decay of the reactive species FADH⁻ and TyrO•.

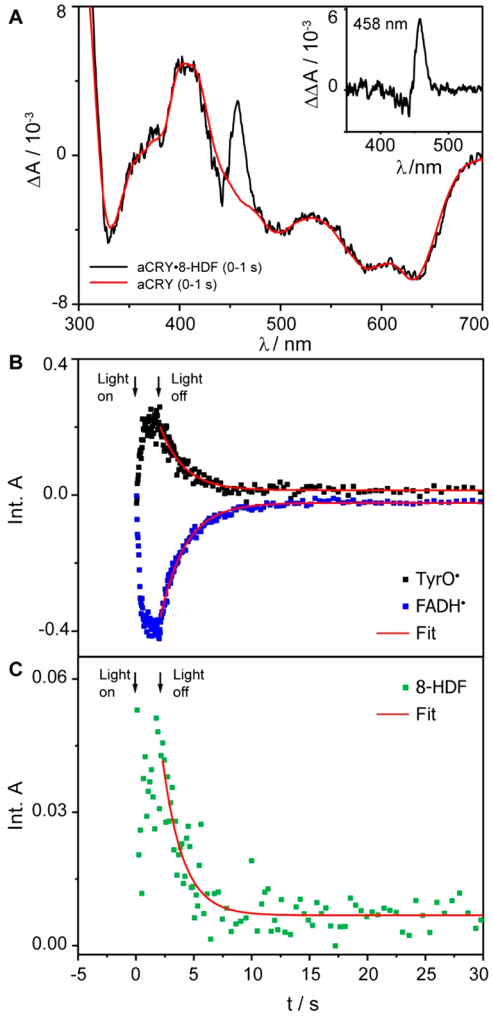

Figure 3. (A) Millisecond time-resolved UV−vis difference spectra of the red-light response in aCRY·8-HDF compared to that in aCRY. The samples were illuminated at 632 nm for 2 s to selectively convert FADH• to FADH⁻. The difference spectrum of aCRY·8-HDF shows an additional band at 458 nm assigned to 8-HDF (inset). (B) The recovery of FADH• and the decay of TyrO• in aCRY·8-HDF were analyzed with monoexponential fits integrating the marker bands at 550−605 and 385−425 nm, respectively, both yielding time constants of 2.0 s. (C) The decay of the integrated 8-HDF band from 450 to 465 nm was fitted monoexponentially yielding a time constant of 1.8 s similar to that of the TyrO•/FADH⁻ decay.

FTIR Spectroscopy. UV−vis spectroscopy of aCRY·8-HDF revealed a transient, red-light-induced change in the absorption coefficient of 8-HDF and a shortening of the lifetime of TyrO• and FADH⁻ relative to that in aCRY. Red-light-induced FTIR difference spectroscopy in the millisecond time regime was conducted on aCRY·8-HDF and aCRY to investigate the origin of these changes on a structural level. Vibrational modes arising from the presence of 8-HDF in aCRY were analyzed using the rapid-scan technique at 10 °C. Spectra of four independent preparations ($\pm 0.11 \times 10^{-4}$ ΔOD at 1557 cm^{-1}) with a time resolution of 70 ms were averaged from 70 ms to 4.1 s and compared to a spectrum of aCRY (nine independent preparations, $\pm 0.25 \times 10^{-4}$ ΔOD at 1557 cm^{-1}) at the same time point taken under identical conditions. Samples were preilluminated with blue light for 10 s to form FADH•. After the detection of a reference spectrum, FADH⁻ was selectively generated by excitation with red light for 3 s followed by the immediate start of data acquisition. The light-induced difference spectrum of aCRY·8-HDF 2 s after illumination shows negative marker bands of FADH• at 1663, 1652, and 1534 cm^{-1} and positive bands from vibrational modes of FADH⁻ at 1623, 1514, 1351, and 1315 cm^{-1} in accordance with the aCRY spectrum (Figure 4A) and literature data.[23,24] The compliant frequencies of the vibrational modes confirm successful red-light-induced generation of FADH⁻ from FADH• in aCRY·8-HDF (Table S2).

Red-Light-Induced Changes in the 8-HDF Protonation State. Vibrational modes arising from the presence of 8-HDF in aCRY were isolated by calculating the double difference spectrum of aCRY·8-HDF minus the aCRY spectrum after scaling the latter to the marker band of FADH⁻ at 1351 cm^{-1} by a factor of 0.51 (Figure 4B). The correct scaling was confirmed by the consistent intensity of multiple positive and negative flavin bands at 1315, 1304, and 1298 cm^{-1} (Figure 4A). DFT calculations of 8-HDF with different protonation states and hydrogen bonding scenarios at the oxygen of the 8-hydroxyl and the carbonyl and amine groups were performed. Difference spectra of these calculations were used for band assignment because previous studies yielded a very good agreement of calculated and experimentally obtained spectra, including the prediction of band shifts in response to changes in hydrogen bonding.[23,32,48−50] The difference spectrum of the deprotonated 8-HDF accepting two hydrogen bonds from two water molecules at the 8-hydroxyl group and a hydrogen bond at the 1-amine and 4-carbonyl group, model 2, minus the protonated 8-HDF accepting a

DOI: 10.1021/acs.biochem.9b00875
Biochemistry 2020, 59, 594−604

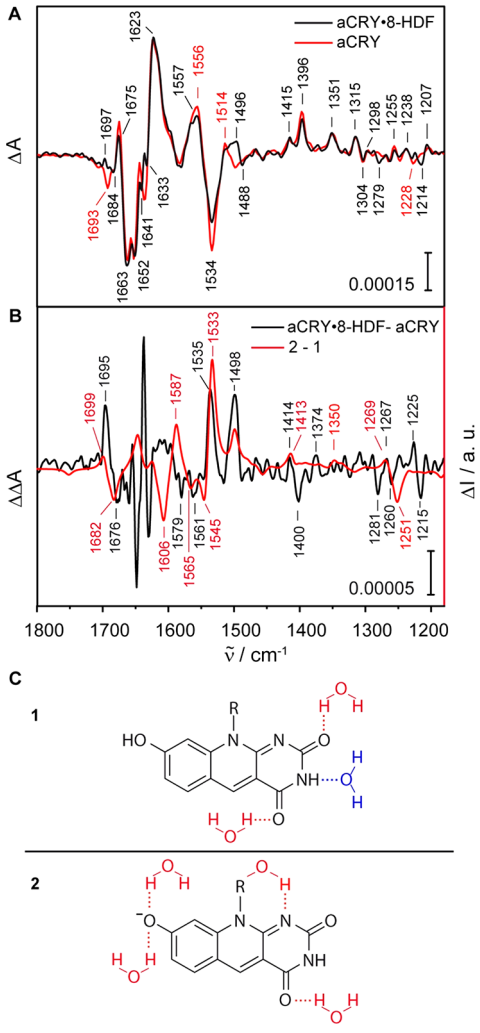

Figure 4. (A) FTIR difference spectra of aCRY·8-HDF and aCRY after red-light illumination. The spectra at 2 s of aCRY·8-HDF (black) and aCRY (red) were averaged from a continuous series of spectra. The latter was scaled by a factor of 0.51 to the marker band of $FADH^-$ at 1351 cm^{-1}. (B) The double difference spectrum of aCRY·8-HDF minus aCRY at 2 s (black) is compared to results of the quantum chemical calculations (red). Signals originate from aCRY and model 1 (negative) and aCRY·8-HDF and model 2 (positive). (C) Chemical structures of the 8-HDF models used in the DFT calculations. In model 1, the 8-hydroxyl group of 8-HDF is protonated, representing the chromophore in the dark state. Model 2 shows the deprotonated 8-hydroxyl group as the acceptor of two hydrogen bonds as assigned to the state after red-light illumination.

hydrogen bond at the 2- and 4-carbonyl group and donating one at the 3-amine group, model 1 (Figure 4C), yielded the best agreement with the experimental data (Figure 4B). On the basis of the comparison of different models as the dark state, a change in the hydrogen bond pattern at the 8-hydroxyl group as the origin for the observed vibrational modes could be ruled out (Figure S4). The assignments were supported by calculating potential energy distributions (Tables S3 and S4). In the calculated spectra, the relative intensities of the bands are not fully representative. The double difference bands from 1660 to 1580 cm^{-1} were omitted from the analysis because of the strong absorption of water in this region.

The negative bands in the experimental spectrum (Figure 4B) originate from modes of either the protonated 8-HDF or the protein matrix exhibiting smaller or negative intensity in the aCRY·8-HDF difference spectrum as compared to aCRY. For the sake of clarity, the following section will discuss only bands attributed to 8-HDF, summarized in Table 1. An assignment of the remaining bands can be found in Table S5.

Table 1. Vibrational Frequencies (cm^{-1}) of 8-HDF Contributions in the aCRY·8-HDF minus aCRY Spectrum Compared to the Calculated Difference Spectrum for Model 2 minus Model 1

aCRY·8-HDF − aCRY			
positive	negative	calculation	assignment
	1676	1682	8-HDF νC_2O[a]
	1579	1565	8-HDF νCC_{ring}, δC_8OH[b]
	1561	1545	8-HDF νCN_{ring}
1535		1533	8-HDF^- νCN_{ring}, νC_8O
1498		1498	8-HDF^- νCC_{ring}, νC_8O
1414		1413	8-HDF^- νCC_{ring}
1267		1269	8-HDF^- $\delta CHH_{ribity\ chain}$
	1260	1251	8-HDF νC_8O

[a] ν = stretching mode. [b] δ = bending mode.

In the experimental spectrum, a negative band at 1676 cm^{-1} is present, which can be assigned to the CO stretching vibration of the 8-HDF 2-carbonyl group found at 1682 cm^{-1} in the calculated spectrum. The two negative bands at 1579 and 1561 cm^{-1} can be assigned to the CC ring and the CN ring stretching mode of the antenna chromophore, respectively. The calculated spectrum also exhibits these features, slightly downshifted at 1565 and 1545 cm^{-1}, respectively. In the protein spectrum, a mode at 1260 cm^{-1} is present, which can be assigned to the 8-hydroxyl CO stretching vibration found at 1251 cm^{-1} in the calculated difference spectrum.

Positive bands in the double difference spectrum arise from either 8-HDF in the deprotonated state or bands with a higher intensity in the aCRY·8-HDF spectrum originating from the protein matrix. The most prominent positive double difference bands in the experimental data are found at 1535 and 1498 cm^{-1} and cannot be assigned to the flavin chromophore or amino acid residues. Although the band at 1535 cm^{-1} is still found within the amide II region, this band is assigned to 8-HDF as in the calculated spectrum a vibrational mode at a similar frequency of 1533 cm^{-1} originating from the CN ring stretching mode and the CO stretching vibration of the deprotonated 8-hydroxyl group is present. The band at 1498 cm^{-1} can unambiguously be assigned to the deprotonated 8-HDF as a mode at the identical position is found in the calculated spectrum, with main contributions from the CO stretching of the 8-hydroxyl group and the CC ring stretching vibration.

The band at 1414 cm^{-1} can be assigned to the CC stretching mode of the 8-HDF ring system, in agreement with the DFT calculations where the band is found at 1413 cm^{-1}. At 1267 cm^{-1}, a small positive mode arises from a CHH bending mode of the ribityl chain as confirmed by a band at 1269 cm^{-1} in the calculated spectrum.

Characteristics of aCRY·8-HDF Fluorescence Emission Depending on the Flavin Oxidation State. Fluorescence spectra of aCRY·8-HDF carrying FAD_{ox} were compared to those of aCRY with FAD_{ox}, deprotonated 8-HDF in a phosphate buffer, and DMSO each with 0.1% Et_3N (Figure

DOI: 10.1021/acs.biochem.9b00875
Biochemistry 2020, 59, 594−604

5A). The fluorescence spectrum of aCRY·8-HDF carrying FAD_{ox} shows a maximum at 459 nm and a shoulder at 489 nm

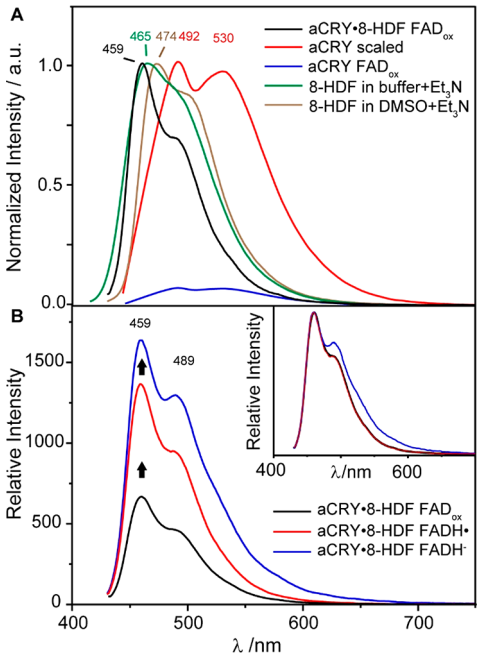

Figure 5. (A) Spectra of aCRY·8-HDF carrying FAD_{ox} are compared to spectra of aCRY with FAD_{ox}, 8-HDF in DMSO with 0.1% Et_3N, and phosphate buffer with 0.1% Et_3N. All data sets are scaled to the emission maximum of aCRY·8-HDF except for the spectra of aCRY with FAD_{ox} (blue). The spectrum of aCRY·8-HDF shows distinct emission bands at 459 and 489 nm blue-shifted compared to those of aCRY with maxima at 492 and 530 nm. (B) Fluorescence spectra of aCRY·8-HDF carrying either FAD_{ox}, $FADH^{\bullet}$, or $FADH^{-}$. FAD_{ox} in aCRY·8-HDF (black) was converted to $FADH^{\bullet}$ (red) by blue-light illumination for 10 s, resulting in a doubling of the fluorescence intensity with no change in the band shape (inset). The reduction of $FADH^{\bullet}$ to $FADH^{-}$ by blue-light illumination for 40 s in the presence of ascorbic acid induces an additional intensity surge of ∼20%.

distinctly blue-shifted compared to the spectrum of aCRY with maxima at 492 and 530 nm. Interestingly, the comparison of the fluorescence intensity of both samples reveals a 10-fold higher intensity of the aCRY·8-HDF emission as compared to that of aCRY. The very weak fluorescence of aCRY with FAD_{ox} (blue curve, Figure 5A) can be explained by the quenching of flavin via ultrafast electron transfer from a neighboring tryptophan.[52] Consequently, the stronger fluorescence and the spectral shift in the aCRY·8-HDF emission spectrum relative to aCRY indicate a predominant fluorescence contribution from 8-HDF.

The spectra of deprotonated 8-HDF in phosphate buffer and DMSO each with 0.1% Et_3N show red-shifted emission maxima at 465 and 474 nm, respectively, presumably as a result of rapid solvation dynamics. To compare the fluorescence yield of aCRY·8-HDF to that of 8-HDF in phosphate buffer with 0.1% Et_3N, the samples were adjusted to the same 8-HDF concentration. The fluorescence intensity of the antenna chromophore in buffer was found to be 13 times higher than that of aCRY·8-HDF with FAD_{ox} (data not shown), implying the quenching of the 8-HDF fluorescence by a resonant energy transfer to flavin as observed previously in photolyases.[34,36,53]

Additionally, the fluorescence of aCRY·8-HDF was investigated as a function of the flavin oxidation state. $FADH^{\bullet}$ was generated upon blue-light illumination for 10 s, and a permanent stabilization of $FADH^{-}$ was achieved upon addition of 10 μM ascorbic acid and blue-light illumination for 40 s (Figure 5B). Upon the conversion of FAD_{ox} to $FADH^{\bullet}$ in aCRY·8-HDF, the fluorescence intensity doubled without a change in the band shape (Figure 5B, inset). In the dark, the fluorescence intensity decreased over time (Figure S2). After conversion of $FADH^{\bullet}$ to $FADH^{-}$, the intensity of fluorescence emission of aCRY·8-HDF increased by 20% and showed a slight increase in the shoulder at 489 nm, indicating a contribution from free flavin due to release upon intense illumination in the presence of ascorbic acid (Figure S5).

The theoretical RET efficiencies for 8-HDF to FAD_{ox}, $FADH^{\bullet}$, and $FADH^{-}$ were calculated to be 99.6%, 99.7%, and 97.0%, respectively. Noticeably, the efficiencies for FAD_{ox} and $FADH^{\bullet}$ are almost identical, which does not explain the experimentally observed increase in fluorescence emission upon $FADH^{\bullet}$ formation.

DISCUSSION

Stabilization of $FADH^{\bullet}$ by the Presence of 8-HDF. Previous work shows that aCRY carries the flavin neutral radical in the dark state of the receptor *in vivo*,[20] although it was found to decay rapidly *in vitro*.[23] To elucidate the impact of the binding of 8-HDF on the stability of $FADH^{\bullet}$, its decay was monitored over a time course of several hours (Figure 2B), revealing an increase in the lifetime major component in aCRY·8-HDF by a factor of 3.5. As the decay of $FADH^{\bullet}$ was shown to be dependent on pH,[23] it was suggested that the deprotonation kinetics is controlled either directly by a neighboring amino acid such as a histidine or indirectly by asparagine 395 functioning as a gatekeeper for a proton transferred from the solvent.[23,29] Evidence for the latter hypothesis is found in the FTIR double difference spectra of aCRY·8-HDF minus aCRY (Figure 4B), showing a prominent positive band at 1695 cm^{-1} close to a position previously assigned in aCRY to red-light-induced changes in the hydrogen bonding of N395.[23,51] We can conclude that the presence of 8-HDF alters the hydrogen bonding network in the flavin-binding pocket, which manifests itself in the stabilization of $FADH^{\bullet}$ and decreases the lifetime of $FADH^{-}$ from 2.6 to 2.0 ms as observed in the UV−vis data (Figures 2B and 3B). This finding is quite unusual, given the chromophore separation of 17.4 Å (center to center) and the lack of obvious structural deviations in the flavin-binding pocket in the crystal structures of aCRY and aCRY·8-HDF.[29] Interestingly, in the 8-HDF-binding pocket, phenylalanine 43 (F43) flips in the presence of 8-HDF to form a $\pi-\pi$ stack with the antenna.[29] This rearrangement could induce alterations in the hydrogen bonding network of the protein spanning a range sufficient to alter the hydrogen bonding network in the flavin-binding pocket. This alteration might also affect the redox potential of flavin, further stabilizing the neutral radical. However, because no structural rearrangements in the flavin-binding pocket are observed in the presence of 8-HDF, the overall effect on the redox potential can be considered as rather small. Nevertheless, to elucidate the impact of the oxygen content of the environment, future studies should test whether the stability of $FADH^{\bullet}$ in aCRY·8-HDF is also irresponsive to changing oxygen levels as observed previously in aCRY.[23]

DOI: 10.1021/acs.biochem.9b00875
Biochemistry 2020, 59, 594−604

From a physiological point of view, the extended lifetime of the neutral radical in the presence of 8-HDF explains how aCRY can fulfill its function as a red-light receptor *in vivo* because $FADH^{\bullet}$ is the only flavin oxidation state with an expanded spectral sensitivity of ≤680 nm. The ability to sense red light is essential for photosynthetic organisms to control adaptive processes. For example, the red-light response enables the organism to detect not only varying light quantities but also qualities. As no phytochrome or other red-light receptor has been identified in *C. reinhardtii* to date,[54] the role of aCRY as a red-light receptor appears to be even more important in this green algae.

Red-Light-Induced Deprotonation of 8-HDF. Millisecond time-resolved UV−vis experiments show an additional absorbance band at 458 nm in the aCRY·8-HDF spectrum, decaying concomitantly with the reactive species $TyrO^{\bullet}$ and $FADH^{-}$. The band at 458 nm is assigned to the red-light-induced bathochromic shift in the 8-HDF absorption by 10 nm (Figure 3A). A similar but even more pronounced red shift is observed upon the deprotonation of 8-HDF in solution where a shift from 390 to 421 nm accompanied by an increase in the molar extinction coefficient is observed,[33,55] indicating the deprotonation of 8-HDF in aCRY·8-HDF upon flavin reduction. Despite the difference in the absorbance maxima of free neutral 8-HDF and 8-HDF bound to aCRY·8-HDF being 60 nm, in the F420-binding protein of *Mycobacterium tuberculosis* the neutral form of the antenna shows an absorbance maximum at 440 nm,[56] revealing the strong impact of the protein environment on the position of the absorbance maximum and supporting the presence of neutral 8-HDF in aCRY·8-HDF. Previously, the strong red shift of the 8-HDF absorbance in photolyases as compared to solution was attributed to a negative solvatochromism as expected for charged species[57] such as the 8-HDF anion in a nonpolar environment in these proteins.[12,35] Compared to other photolyases carrying 8-HDF, in aCRY·8-HDF the absorption shift is especially pronounced with a maximum found at 448 nm.[29,36] Only the (6−4) photolyase of *Drosophila melanogaster* shows a similar shift to the red,[10,36] implying that both 8-HDF-binding pockets harbor similar nonpolar amino acids. However, in aCRY·8-HDF, F43 forms a $\pi-\pi$ stack with 8-HDF providing a logical origin for the red shift, whereas the corresponding amino acid in (6−4) *D. melanogaster* is isoleucine 50. Furthermore, in the *Methanosarcina mazei* CPD photolyase, phenylalanine 61 is also found in a $\pi-\pi$ stack without causing a red shift (A_{max} = 435 nm).[36] Interestingly, in this protein, the exchange of the polar serine 26 with the nonpolar leucine induced a blue shift of the absorbance to 432 nm, hinting at a positive solvatochromism instead. The respective amino acid at this position sensitive to changes in the polarity in aCRY·8-HDF and the *D. melanogaster* (6−4) photolyase is a positively charged arginine (R12 and R13, respectively). This supports the theory of a positive solvatochromic effect and the assignment of the red-shift in the 8-HDF absorption to the formation of the 8-HDF anion.

This theory is supported by the comparison of the FTIR data with DFT calculations of 8-HDF at different protonation states, which allowed the assignment of the bands at 1535 and 1498 cm^{-1} to the CO stretching vibration of the 8-HDF anion. For the modeling of the negative bands of the experimental data, a calculated spectrum of the protonated 8-HDF gave the best results. Here, the COH bending vibration of the hydroxyl group and a CN ring stretching mode, found at 1565 and 1545 cm^{-1}, respectively, are slightly downshifted compared to the bands from the experimental data found at 1579 and 1561 cm^{-1}. The downshift can be attributed to the complex environment of the hydroxyl group in the antenna-binding pocket that might not be completely mimicked in the calculations. In the two models, the hydrogen bonding structures of the carbonyl and amine groups of 8-HDF also differ, indicating overall changes in the hydrogen bonding network in the antenna-binding pocket. Finally, the very good agreement of the calculated difference spectrum of deprotonated 8-HDF^{-} minus protonated 8-HDF with the experimental data supports the theory of the red-light-induced deprotonation of the antenna, indicating a long-range coupling of the chromophores via the hydrogen bonding network.

Energy Transfer Processes in aCRY·8-HDF Depending on the Flavin Oxidation State. To date, energy transfer processes in cryptochromes have not been studied extensively. Here, we investigated this phenomenon in a cryptochrome carrying FAD and 8-HDF. The fluorescence emission spectrum of aCRY·8-HDF shows an intensity 13-fold lower than that of 8-HDF solvated in phosphate buffer, resulting from the quenching via RET between flavin and 8-HDF in aCRY·8-HDF as observed previously in photolyases[34,53] and the *Vibrio cholerae* cryptochrome *Vc*Cry1 between FAD and MTHF.[58]

Remarkably, a doubling of the fluorescence yield occurred upon light-induced conversion from FAD_{ox} to $FADH^{\bullet}$, followed by an additional intensity surge upon $FADH^{-}$ formation (Figure 5B). Interestingly, only for the conversion from $FADH^{\bullet}$ to $FADH^{-}$ was a similar phenomenon reported for *A. nidulans* (6−4) and *E. coli* photolyases.[34,53,59] The observed intensity surge upon $FADH^{-}$ formation is not completely in agreement with the results of the efficiency calculations, where a difference of around 4% is predicted opposed to 20% in our experimental spectra. Interestingly, a similar increase in fluorescence intensity was observed for solvated 8-HDF upon its deprotonation,[33] giving further evidence of the deprotonation of the antenna upon flavin reduction in aCRY·8-HDF. Overall, the calculated RET efficiency of 97.0% for $FADH^{-}$ is in a range of previously determined transfer efficiencies of photolyases of 99.6% and 92%.[45,53] However, the intensity surge observed upon conversion from FAD_{ox} to $FADH^{\bullet}$ is not reflected by the calculations and has not been observed before. Again, this phenomenon can be explained by the increase in fluorescence intensity upon 8-HDF deprotonation, indicating that in some proteins 8-HDF is already deprotonated upon $FADH^{\bullet}$ formation. In addition, changes in the orientation factor κ^2 upon 8-HDF deprotonation and flavin reduction might contribute to this phenomenon. In the *E. coli* photolyase, it was shown that the reduction of FAD_{ox} to $FADH^{\bullet}$ and $FADH^{-}$ led to significant changes in κ^2 caused by alterations in the transition dipole moment.[59] Considering that 8-HDF might be partially deprotonated upon $FADH^{\bullet}$ formation, the transition dipole moment of 8-HDF will also change. In that case, κ^2 might be altered even more drastically, resulting in changes in RET efficiencies. To verify this theory, time-dependent density functional theory for the determination of the transition dipole moments could be employed.

Even upon $FADH^{-}$ formation, the fluorescence intensity of solvated 8-HDF is still 6 times higher. Nevertheless, in aCRY·8-HDF, the fluorescence intensity is not as strongly reduced as

DOI: 10.1021/acs.biochem.9b00875
Biochemistry 2020, 59, 594−604

in 8-HDF-binding photolyases such as the *A. nidulans* (6–4) photolyase, where a 25-fold decrease is observed,[34,60] indicating a less efficient energy transfer between 8-HDF and $FADH^-$ in aCRY·8-HDF. Due to an additional purification step of the samples prior to the experiments, the contribution from the free chromophore as a source for the higher intensity can be ruled out. Because aCRY·8-HDF has a dual function as a red-light receptor as well as a (6–4) photolyase, the reduced energy transfer efficiency might help to keep the balance between overexcitation when acting as a red-light receptor and DNA repair efficiency when acting as a photolyase. The change in the transfer efficiency depending on the flavin oxidation state could be used by the protein to further regulate the amount of light energy needed for the respective task. Picosecond transient absorption spectroscopy might help to reveal the dissipation pathways of the transferred light energy.

CONCLUSIONS

In this study, the essential role of the antenna pigment 8-HDF for the functionality of the bifunctional cryptochrome aCRY beyond the sole purpose of light harvesting is disclosed. The binding of 8-HDF at a 17.4 Å distance to the flavin significantly stabilizes the dark state of the receptor, $FADH^•$, *in vitro*. Changes in the hydrogen bonding network of N395 in the flavin-binding pocket are responsible for the effect as evidenced by FTIR spectroscopy. Upon red-light excitation of $FADH^•$, 8-HDF shows a red-shift in UV–vis absorption concomitant with the formation and decay of the reactive species, $FADH^-$ and $TyrO^•$. On the basis of the presented FTIR spectra and quantum chemical calculations, we propose the changes to originate from the deprotonation of 8-HDF upon $FADH^-$ formation, questioning the paradigm of 8-HDF as being permanently bound in its deprotonated state in cryptochromes and photolyases. Investigation of the energy transfer processes revealed a drastic decrease in the transfer efficiency of 8-HDF upon flavin reduction, likely linked to the deprotonation of 8-HDF, a phenomenon not observed before and possibly responsible for the balancing of aCRY's dual function.

Here, the interdependence of an antenna pigment and a light-sensing chromophore via a long-range hydrogen bonding network is presented and supported by experimental and theoretical data. In aCRY·8-HDF, this coupling is found to be essential for the protein's function as a red-light receptor and we suggest this connection also regulates the efficiency of energy transfer from 8-HDF to flavin. This represents an effective mechanism for controlling the activation of aCRY and possibly facilitating the dual function as both a photolyase and a red-light receptor. Because several bifunctional cryptochromes are currently known,[61–65] this concept represents a plausible strategy also employed by other members of this protein family.

ASSOCIATED CONTENT

Supporting Information

The Supporting Information is available free of charge at https://pubs.acs.org/doi/10.1021/acs.biochem.9b00875.

Material and Methods, describing size exclusion chromoptography. Results, including assignment of vibrational modes arising from changes in the hydrogen bonding network of asparagine 395 and tyrosine 373; discussion of the band assignment of tyrosine 373; absorbance spectra of aCRY·8-HDF after size exclusion chromatography (Figure S1); fluorescence emission spectra (Figure S2); alternative chemical structures and DFT calculations (Figure S3); overlap integral used to calculate the Foerster efficiency (Figure S4); difference spectrum of the scaled fluorescence emission of aCRY·8-HDF (Figure S5); optimized structure of the deprotonated 8-hydroxy-5-deazaflavin (Figure S6); parameters used to calculate the Foerster resonance energy transfer efficiencies (Table S1); assignment of the FTIR difference bands of aCRY·8-HDF and aCRY after the conversion of $FADH^•$ to $FADH^-$ (Table S2); PED analysis of 8-HDF (Table S3); PED analysis of the 8-HDF anion (Table S4); and assignment of vibrational modes originating from the residues asparagine 395 and tyrosine 373 (Table S5) (PDF)

Accession Codes

UniProt entry A8J8W0.

AUTHOR INFORMATION

Corresponding Author

*E-mail: soldemeyer@lbl.gov.

ORCID

Sabine Oldemeyer: 0000-0001-7139-7218

Author Contributions

S.O. designed the study. S.O. performed and analyzed the experiments with advice from G.R.F. and A.Z.H. S.O. wrote the manuscript with advice from A.Z.H. and G.R.F. All authors have approved the final version of the manuscript.

Funding

This work was supported by the Deutsche Forschungsgemeinschaft (DFG) via DFG Grant OL555/1-1 to S.O. The quantum chemical calculations were performed with the support of National Institutes of Health Grant S10OD023532. A.Z.H. was supported by the Department of Energy Solar Energy Technologies Office (Grant DE-EE00032324). G.R.F. was supported by the U.S. Department of Energy, Office of Science, Basic Energy Sciences, Chemical Sciences, Geosciences, and Biosciences Division.

Notes

The authors declare no competing financial interest.

ACKNOWLEDGMENTS

The authors thank Tilman Kottke and Christian Thöing for their support and Jens Christoffers for providing synthetic 8-HDF.

ABBREVIATIONS

8-HDF, 8-hydroxy-5-deazaflavin; *Cra*CRY, *C. reinhardtii* animal-like cryptochrome; DFT, density functional theory; DMLR, 6,7-dimethyl-8-ribityllumazine; FAD, flavin adenine dinucleotide; $FADH^•$, flavin neutral radical; $FADH^-$, flavin fully reduced state; FTIR, Fourier transform infrared; FMN, flavin mononucleotide; MTHF, 5,10-methenyltetrahydrofolate; PHR, photolyase homology region.

REFERENCES

(1) Sancar, A. (2003) Structure and function of DNA photolyase and cryptochrome blue-light photoreceptors. *Chem. Rev. 103*, 2203–2237.

DOI: 10.1021/acs.biochem.9b00875
Biochemistry 2020, 59, 594–604

(2) Losi, A., and Gärtner, W. (2012) The evolution of flavin-binding photoreceptors: an ancient chromophore serving trendy blue-light sensors. *Annu. Rev. Plant Biol. 63*, 49−72.
(3) Chaves, I., Pokorny, R., Byrdin, M., Hoang, N., Ritz, T., Brettel, K., Essen, L. O., van der Horst, G. T., Batschauer, A., and Ahmad, M. (2011) The cryptochromes: blue light photoreceptors in plants and animals. *Annu. Rev. Plant Biol. 62*, 335−364.
(4) Lin, C., and Shalitin, D. (2003) Cryptochrome structure and signal transduction. *Annu. Rev. Plant Biol. 54*, 469−496.
(5) Hore, P. J., and Mouritsen, H. (2016) The Radical-Pair Mechanism of Magnetoreception. *Annu. Rev. Biophys. 45*, 299−344.
(6) Rupert, C. S. (1960) Photoreactivation of transforming DNA by an enzyme from bakers' yeast. *J. Gen. Physiol. 43*, 573−595.
(7) Todo, T., Takemori, H., Ryo, H., Ihara, M., Matsunaga, T., Nikaido, O., Sato, K., and Nomura, T. (1993) A new photoreactivating enzyme that specifically repairs ultraviolet light-induced (6−4) photoproducts. *Nature 361*, 371−374.
(8) Johnson, J. L., Hamm-Alvarez, S., Payne, G., Sancar, G. B., Rajagopalan, K. V., and Sancar, A. (1988) Identification of the second chromophore of *Escherichia coli* and yeast DNA photolyases as 5,10-methenyltetrahydrofolate. *Proc. Natl. Acad. Sci. U. S. A. 85*, 2046−2050.
(9) Klar, T., Pokorny, R., Moldt, J., Batschauer, A., and Essen, L. O. (2007) Cryptochrome 3 from *Arabidopsis thaliana*: structural and functional analysis of its complex with a folate light antenna. *J. Mol. Biol. 366*, 954−964.
(10) Glas, A. F., Maul, M. J., Cryle, M., Barends, T. R., Schneider, S., Kaya, E., Schlichting, I., and Carell, T. (2009) The archaeal cofactor F0 is a light-harvesting antenna chromophore in eukaryotes. *Proc. Natl. Acad. Sci. U. S. A. 106*, 11540−11545.
(11) Selby, C. P., and Sancar, A. (2012) The second chromophore in *Drosophila* photolyase/cryptochrome family photoreceptors. *Biochemistry 51*, 167−171.
(12) Eker, A. P., Kooiman, P., Hessels, J. K., and Yasui, A. (1990) DNA photoreactivating enzyme from the cyanobacterium Anacystis nidulans. *J. Biol. Chem. 265*, 8009−8015.
(13) Ueda, T., Kato, A., Kuramitsu, S., Terasawa, H., and Shimada, I. (2005) Identification and characterization of a second chromophore of DNA photolyase from *Thermus thermophilus* HB27. *J. Biol. Chem. 280*, 36237−36243.
(14) Geisselbrecht, Y., Frühwirth, S., Schroeder, C., Pierik, A. J., Klug, G., and Essen, L. O. (2012) CryB from *Rhodobacter sphaeroides*: a unique class of cryptochromes with new cofactors. *EMBO Rep. 13*, 223−229.
(15) Fujihashi, M., Numoto, N., Kobayashi, Y., Mizushima, A., Tsujimura, M., Nakamura, A., Kawarabayasi, Y., and Miki, K. (2007) Crystal structure of archaeal photolyase from *Sulfolobus tokodaii* with two FAD molecules: implication of a novel light-harvesting cofactor. *J. Mol. Biol. 365*, 903−910.
(16) Yang, H. Q., Wu, Y. J., Tang, R. H., Liu, D., Liu, Y., and Cashmore, A. R. (2000) The C termini of *Arabidopsis* cryptochromes mediate a constitutive light response. *Cell 103*, 815−827.
(17) Kutta, R. J., Archipowa, N., and Scrutton, N. S. (2018) The sacrificial inactivation of the blue-light photosensor cryptochrome from Drosophila melanogaster. *Phys. Chem. Chem. Phys. 20*, 28767−28776.
(18) Kottke, T., Oldemeyer, S., Wenzel, S., Zou, Y., and Mittag, M. (2017) Cryptochrome photoreceptors in green algae: Unexpected versatility of mechanisms and functions. *J. Plant Physiol. 217*, 4−14.
(19) Fortunato, A. E., Annunziata, R., Jaubert, M., Bouly, J. P., and Falciatore, A. (2015) Dealing with light: The widespread and multitasking cryptochrome/photolyase family in photosynthetic organisms. *J. Plant Physiol. 172C*, 42−54.
(20) Beel, B., Prager, K., Spexard, M., Sasso, S., Weiss, D., Müller, N., Heinnickel, M., Dewez, D., Ikoma, D., Grossman, A. R., Kottke, T., and Mittag, M. (2012) A Flavin Binding Cryptochrome Photoreceptor Responds to Both Blue and Red Light in *Chlamydomonas reinhardtii*. *Plant Cell 24*, 2992−3008.
(21) Bouly, J. P., Schleicher, E., Dionisio-Sese, M., Vandenbussche, F., Van Der Straeten, D., Bakrim, N., Meier, S., Batschauer, A., Galland, P., Bittl, R., and Ahmad, M. (2007) Cryptochrome blue light photoreceptors are activated through interconversion of flavin redox states. *J. Biol. Chem. 282*, 9383−9391.
(22) Banerjee, R., Schleicher, E., Meier, S., Viana, R. M., Pokorny, R., Ahmad, M., Bittl, R., and Batschauer, A. (2007) The signaling state of *Arabidopsis* cryptochrome 2 contains flavin semiquinone. *J. Biol. Chem. 282*, 14916−14922.
(23) Spexard, M., Thöing, C., Beel, B., Mittag, M., and Kottke, T. (2014) Response of the Sensory Animal-like Cryptochrome aCRY to Blue and Red Light As Revealed by Infrared Difference Spectroscopy. *Biochemistry 53*, 1041−1050.
(24) Oldemeyer, S., Franz, S., Wenzel, S., Essen, L. O., Mittag, M., and Kottke, T. (2016) Essential Role of an Unusually Long-lived Tyrosyl Radical in the Response to Red Light of the Animal-like Cryptochrome aCRY. *J. Biol. Chem. 291*, 14062−14071.
(25) Franz-Badur, S., Penner, A., Straß, S., von Horsten, S., Linne, U., and Essen, L.-O. (2019) Structural changes within the bifunctional cryptochrome/photolyase CraCRY upon blue light excitation. *Sci. Rep. 9*, 9896−9896.
(26) Berndt, A., Kottke, T., Breitkreuz, H., Dvorsky, R., Hennig, S., Alexander, M., and Wolf, E. (2007) A novel photoreaction mechanism for the circadian blue light photoreceptor *Drosophila* cryptochrome. *J. Biol. Chem. 282*, 13011−13021.
(27) Immeln, D., Schlesinger, R., Heberle, J., and Kottke, T. (2007) Blue light induces radical formation and autophosphorylation in the light-sensitive domain of *Chlamydomonas* cryptochrome. *J. Biol. Chem. 282*, 21720−21728.
(28) Müller, P., and Ahmad, M. (2011) Light-activated Cryptochrome Reacts with Molecular Oxygen to Form a Flavin-Superoxide Radical Pair Consistent with Magnetoreception. *J. Biol. Chem. 286*, 21033−21040.
(29) Franz, S., Ignatz, E., Wenzel, S., Zielosko, H., Putu, E. P. G. N., Maestre-Reyna, M., Tsai, M.-D., Yamamoto, J., Mittag, M., and Essen, L.-O. (2018) Structure of the bifunctional cryptochrome aCRY from Chlamydomonas reinhardtii. *Nucleic Acids Res. 46*, 8010−8022.
(30) Lacombat, F., Espagne, A., Dozova, N., Plaza, P., Müller, P., Brettel, K., Franz-Badur, S., and Essen, L.-O. (2019) Ultrafast Oxidation of a Tyrosine by Proton-Coupled Electron Transfer Promotes Light Activation of an Animal-like Cryptochrome. *J. Am. Chem. Soc. 141*, 13394−13409.
(31) Nohr, D., Franz, S., Rodriguez, R., Paulus, B., Essen, L. O., Weber, S., and Schleicher, E. (2016) Extended Electron-Transfer in Animal Cryptochromes Mediated by a Tetrad of Aromatic Amino Acids. *Biophys. J. 111*, 301−311.
(32) Oldemeyer, S., Mittag, M., and Kottke, T. (2019) Time-Resolved Infrared and Visible Spectroscopy on Cryptochrome aCRY: Basis for Red Light Reception. *Biophys. J. 117*, 490−499.
(33) Eirich, L. D., Vogels, G. D., and Wolfe, R. S. (1979) Distribution of coenzyme F420 and properties of its hydrolytic fragments. *J. Bacteriol. 140*, 20−27.
(34) Malhotra, K., Kim, S. T., Walsh, C., and Sancar, A. (1992) Roles of FAD and 8-hydroxy-5-deazaflavin chromophores in photoreactivation by Anacystis nidulans DNA photolyase. *J. Biol. Chem. 267*, 15406−15411.
(35) Jacobson, F., and Walsh, C. (1984) Properties of 7,8-didemethyl-8-hydroxy-5-deazaflavins relevant to redox coenzyme function in methanogen metabolism. *Biochemistry 23*, 979−988.
(36) Kiontke, S., Gnau, P., Haselsberger, R., Batschauer, A., and Essen, L. O. (2014) Structural and Evolutionary Aspects of Antenna Chromophore Usage by Class II Photolyases. *J. Biol. Chem. 289*, 19659−19669.
(37) Swinehart, D. F. (1962) The Beer-Lambert Law. *J. Chem. Educ. 39*, 333.
(38) Siegel, L. M. (1978) Quantitative determination of non-covalently bound flavins: types and methods of analysis. *Methods Enzymol. 53*, 419−429.

DOI: 10.1021/acs.biochem.9b00875
Biochemistry 2020, 59, 594−604

(39) Artimo, P., Jonnalagedda, M., Arnold, K., Baratin, D., Csardi, G., de Castro, E., Duvaud, S., Flegel, V., Fortier, A., Gasteiger, E., Grosdidier, A., Hernandez, C., Ioannidis, V., Kuznetsov, D., Liechti, R., Moretti, S., Mostaguir, K., Redaschi, N., Rossier, G., Xenarios, I., and Stockinger, H. (2012) ExPASy: SIB bioinformatics resource portal. *Nucleic Acids Res. 40*, W597−603.
(40) Frisch, M. J., Trucks, G. W., Schlegel, H. B., Scuseria, G. E., Robb, M. A., Cheeseman, J. R., Scalmani, G., Barone, V., Petersson, G. A., Nakatsuji, H., Li, X., Caricato, M., Marenich, A. V., Bloino, J., Janesko, B. G., Gomperts, R., Mennucci, B., Hratchian, H. P., Ortiz, J. V., Izmaylov, A. F., Sonnenberg, J. L., Williams, Ding, F., Lipparini, F., Egidi, F., Goings, J., Peng, B., Petrone, A., Henderson, T., Ranasinghe, D., Zakrzewski, V. G., Gao, J., Rega, N., Zheng, G., Liang, W., Hada, M., Ehara, M., Toyota, K., Fukuda, R., Hasegawa, J., Ishida, M., Nakajima, T., Honda, Y., Kitao, O., Nakai, H., Vreven, T., Throssell, K., Montgomery, J. A., Jr., Peralta, J. E., Ogliaro, F., Bearpark, M. J., Heyd, J. J., Brothers, E. N., Kudin, K. N., Staroverov, V. N., Keith, T. A., Kobayashi, R., Normand, J., Raghavachari, K., Rendell, A. P., Burant, J. C., Iyengar, S. S., Tomasi, J., Cossi, M., Millam, J. M., Klene, M., Adamo, C., Cammi, R., Ochterski, J. W., Martin, R. L., Morokuma, K., Farkas, O., Foresman, J. B., and Fox, D. J. (2016) *Gaussian 16*, revision A.03, Gaussian, Inc., Wallingford, CT.
(41) Becke, A. D. (1993) Density-functional thermochemistry. III. The role of exact exchange. *J. Chem. Phys. 98*, 5648−5652.
(42) Stephens, P. J., Devlin, F. J., Chabalowski, C. F., and Frisch, M. J. (1994) Ab Initio Calculation of Vibrational Absorption and Circular Dichroism Spectra Using Density Functional Force Fields. *J. Phys. Chem. 98*, 11623−11627.
(43) Thöing, C., Pfeifer, A., Kakorin, S., and Kottke, T. (2013) Protonated triplet-excited flavin resolved by step-scan FTIR spectroscopy: implications for photosensory LOV domains. *Phys. Chem. Chem. Phys. 15*, 5916−5926.
(44) Spexard, M., Immeln, D., Thöing, C., and Kottke, T. (2011) Infrared spectrum and absorption coefficient of the cofactor flavin in water. *Vib. Spectrosc. 57*, 282−287.
(45) Zheng, X., Garcia, J., and Stuchebrukhov, A. A. (2008) Theoretical Study of Excitation Energy Transfer in DNA Photolyase. *J. Phys. Chem. B 112*, 8724−8729.
(46) Tamada, T., Kitadokoro, K., Higuchi, Y., Inaka, K., Yasui, A., de Ruiter, P. E., Eker, A. P., and Miki, K. (1997) Crystal structure of DNA photolyase from *Anacystis nidulans*. *Nat. Struct. Mol. Biol. 4*, 887−891.
(47) Kim, S. T., Heelis, P. F., Okamura, T., Hirata, Y., Mataga, N., and Sancar, A. (1991) Determination of rates and yields of interchromophore (folate−>flavin) energy transfer and intermolecular (flavin−>DNA) electron transfer in Escherichia coli photolyase by time-resolved fluorescence and absorption spectroscopy. *Biochemistry 30*, 11262−11270.
(48) Rieff, B., Mathias, G., Bauer, S., and Tavan, P. (2011) Density functional theory combined with molecular mechanics: the infrared spectra of flavin in solution. *Photochem. Photobiol. 87*, 511−523.
(49) Martin, C. B., Tsao, M.-L., Hadad, C. M., and Platz, M. S. (2002) The Reaction of Triplet Flavin with Indole. A Study of the Cascade of Reactive Intermediates Using Density Functional Theory and Time Resolved Infrared Spectroscopy. *J. Am. Chem. Soc. 124*, 7226−7234.
(50) Takahashi, R., Okajima, K., Suzuki, H., Nakamura, H., Ikeuchi, M., and Noguchi, T. (2007) FTIR study on the hydrogen bond structure of a key tyrosine residue in the flavin-binding blue light sensor TePixD from *Thermosynechococcus elongatus*. *Biochemistry 46*, 6459−6467.
(51) Iwata, T., Zhang, Y., Hitomi, K., Getzoff, E. D., and Kandori, H. (2010) Key Dynamics of Conserved Asparagine in a Cryptochrome/Photolyase Family Protein by Fourier Transform Infrared Spectroscopy. *Biochemistry 49*, 8882−8891.
(52) Immeln, D., Weigel, A., Kottke, T., and Pérez Lustres, J. L. (2012) Primary events in the blue light sensor plant cryptochrome: intraprotein electron and proton transfer revealed by femtosecond spectroscopy. *J. Am. Chem. Soc. 134*, 12536−12546.
(53) Kim, S. T., Heelis, P. F., and Sancar, A. (1992) Energy transfer (deazaflavin−>FADH2) and electron transfer (FADH2 −>T<>T) kinetics in Anacystis nidulans photolyase. *Biochemistry 31*, 11244−11248.
(54) Mittag, M., Kiaulehn, S., and Johnson, C. H. (2005) The circadian clock in *Chlamydomonas reinhardtii*. What is it for? What is it similar to? *Plant Physiol. 137*, 399−409.
(55) Mohamed, A. E., Ahmed, F. H., Arulmozhiraja, S., Lin, C. Y., Taylor, M. C., Krausz, E. R., Jackson, C. J., and Coote, M. L. (2016) Protonation state of F420H2 in the prodrug-activating deazaflavin dependent nitroreductase (Ddn) from Mycobacterium tuberculosis. *Mol. BioSyst. 12*, 1110−1113.
(56) Bashiri, G., Perkowski, E. F., Turner, A. P., Feltcher, M. E., Braunstein, M., and Baker, E. N. (2012) Tat−Dependent Translocation of an F420−Binding Protein of Mycobacterium tuberculosis. *PLoS One 7*, No. e45003.
(57) Reichardt, C. (1994) Solvatochromic Dyes as Solvent Polarity Indicators. *Chem. Rev. 94*, 2319−2358.
(58) Saxena, C., Wang, H., Kavakli, I. H., Sancar, A., and Zhong, D. (2005) Ultrafast dynamics of resonance energy transfer in cryptochrome. *J. Am. Chem. Soc. 127*, 7984−7985.
(59) Tan, C., Guo, L., Ai, Y., Li, J., Wang, L., Sancar, A., Luo, Y., and Zhong, D. (2014) Direct Determination of Resonance Energy Transfer in Photolyase: Structural Alignment for the Functional State. *J. Phys. Chem. A 118*, 10522−10530.
(60) Kort, R., Komori, H., Adachi, S.-i., Miki, K., and Eker, A. (2004) DNA apophotolyase from Anacystis nidulans: 1.8 A structure, 8-HDF reconstitution and X-ray-induced FAD reduction. *Acta Crystallogr., Sect. D: Biol. Crystallogr. 60*, 1205−1213.
(61) Coesel, S., Mangogna, M., Ishikawa, T., Heijde, M., Rogato, A., Finazzi, G., Todo, T., Bowler, C., and Falciatore, A. (2009) Diatom PtCPF1 is a new cryptochrome/photolyase family member with DNA repair and transcription regulation activity. *EMBO Rep. 10*, 655−661.
(62) García-Esquivel, M., Esquivel-Naranjo, E. U., Hernández-Onate, M. A., Ibarra-Laclette, E., and Herrera-Estrella, A. (2016) The *Trichoderma atroviride* cryptochrome/photolyase genes regulate the expression of blr1-independent genes both in red and blue light. *Fungal Biol. 120*, 500−512.
(63) Heijde, M., Zabulon, G., Corellou, F., Ishikawa, T., Brazard, J., Usman, A., Sanchez, F., Plaza, P., Martin, M., Falciatore, A., Todo, T., Bouget, F. Y., and Bowler, C. (2010) Characterization of two members of the cryptochrome/photolyase family from *Ostreococcus tauri* provides insights into the origin and evolution of cryptochromes. *Plant, Cell Environ. 33*, 1614−1626.
(64) Selby, C. P., and Sancar, A. (2006) A cryptochrome/photolyase class of enzymes with single-stranded DNA-specific photolyase activity. *Proc. Natl. Acad. Sci. U. S. A. 103*, 17696−17700.
(65) Pokorny, R., Klar, T., Hennecke, U., Carell, T., Batschauer, A., and Essen, L. O. (2008) Recognition and repair of UV lesions in loop structures of duplex DNA by DASH-type cryptochrome. *Proc. Natl. Acad. Sci. U. S. A. 105*, 21023−21027.

DOI: 10.1021/acs.biochem.9b00875
Biochemistry 2020, 59, 594−604